Journal of Thermal Analysis, Vol. 46 (1996) 1177-1189

Dedicated to Professor Bernhard Wunderlich on the occasion of his 65th birthday

THERMOPOROSIMETRY
Pore size distribution measurements for microporous glass using differential scanning calorimetry

K. Ishikiriyama[1*], *M. Todoki*[1], *K. H. Min*[2], *S. Yonemori*[2] *and M. Noshiro*[2]

[1]Toray Research Center, Inc., Sonoyama 3-3-7, Otsu, Shiga, 520, Japan
[2]Asahi Glass, Co. Ltd., Hasawa-Cho 1150, Kanagawa-Ku, Yokohama, Kanagawa, 221, Japan

Abstract

The pore size distributions (PSDs) of microporous glass, which were controlled by acid leaching subsequent to phase separation of $CaO–Al_2O_3–B_2O_3–SiO_2$ glass, were determined via both mercury porosimetry and thermoporosimetry (thermal porosimetry). As a result, the pore radii, the cumulative pore volumes, and the surface areas determined via thermoporosimetry were in good agreement with those determined via mercury porosimetry. It was revealed that thermoporosimetry could be applied to pore structure analysis for porous materials having pore sizes at least up to 58 nm in radius.

Keywords: DSC, mercury porosimetry, pore size distribution, porous glass, thermoporosimetry, water

Introduction

Thermoporosimetry (thermal porosimetry) is a technique for determining the pore size distribution (PSD) of a porous material from the melting and freezing curves of liquid, conventionally water, confined in the pores. This has been accomplished by the determination of the thickness of nonfreezable pore water with an optimization using differential scanning calorimetry (DSC) [1, 2]. The detailed procedure regarding the transformation into the PSD from the distribution of the freezing or melting temperature has previously been reported in the literature [1, 2].

By applying thermoporosimetry to 12 kinds of commercial silica gels, the peak radii of the PSD, the pore volumes, and the surface areas obtained via

* To whom all correspondence should be addressed.

0368–4466/96/ $ 5.00

John Wiley & Sons, Limited
Chichester

thermoporosimetry were found to be consistent with those obtained via both nitrogen gas adsorption-desorption and mercury penetration porosimetry [2].

In addition to the silica gels, thermoporosimetry was applied to hydrogel-hollow-fiber membranes for artificial kidneys such as poly(methyl methacrylate) (PMMA), cellulose triacetate (CTA), polyacrylonitrile (PAN), and polysulfone (PS) [3, 4]. For PMMA membranes, the average pore radii obtained via thermoporosimetry have proved to be in good agreement with those obtained via water permeability on the basis of hydrodynamics [3]. The PSD curves of the PMMA membranes were also found to change before and after freeze-drying. As far as the freeze-dryed samples of PMMA, CTA, PAN, and PS membranes are concerned, the pore structures determined via thermoporosimetry were consistent with those determined via nitrogen gas adsorption-desorption [4].

In this study, the pore structure of microporous glass (MPG, registered trademark of Asahi Glass) was investigated using both thermoporosimetry and mercury penetration porosimetry. The PSD is known to be narrow because of the controllable pore structure manufactured from $CaO–Al_2O_3–B_2O_3–SiO_2$ glass by phase separation and acid leaching [5]. The comparisons of the pore radii, the pore volumes, and the surface areas of MPG obtained via both porosimetries are reported.

Experimental techniques

Preparation of samples

Eleven types of MPG as given in Table 1 were manufactured by Asahi Glass, Co. Ltd. The manufacturing process for MPG was as follows [5]: At first, the primary glass, $CaO–Al_2O_3–B_2O_3–SiO_2$, was made and formed into a plate or tube. The primary glass was heated at 600 to 750°C for several hours. This treatment caused the homogeneous primary glass to undergo phase separation into a $SiO_2–Al_2O_3$ rich glass and a $CaO–B_2O_3$ phase. The latter is easily dissolved in acid. The desired MPG was obtained by immersing this heated primary glass into dilute hydrochloric acid. The samples were broken into pieces, and the samples that passed a net of 80/120 mesh (177~125 μm), except for MPG80, were used for thermoporosimetry and mercury porosimetry. For MPG80, blocks of 1–2 mm size prepared by breaking a hollow tube were used for the porosimetries. The average pore radius, R_m, which is defined by $2V_m/S_m$ (where V_m is the pore volume and S_m is the surface area), determined via mercury porosimetry ranged from 6 to 58 nm.

Mercury penetration measurements

After drying the samples under vacuum at room temperature for 15 min, the mercury penetration porosimetry of ca. 500 mg samples was carried out using a Carlo Erba penetration porosimeter Model 220.

Scanning electron microscopy

The samples of MPG300 and MPG475 were examined in a Hitachi S-900 ultra-high-resolution scanning microscope (UHR SEM). Each specimen was lightly coated with platinum before being placed in the microscope.

Figure 1 shows two representative micrographs (a, b) of MPG. The pores are voids formed by dissolution of the $CaO–B_2O_3$ phase. The width of the $Al_2O_3–SiO_2$ matrix in MPG475 was thinner than that in MPG300, and hence the size of the pores of MPG475 was larger than of MPG300.

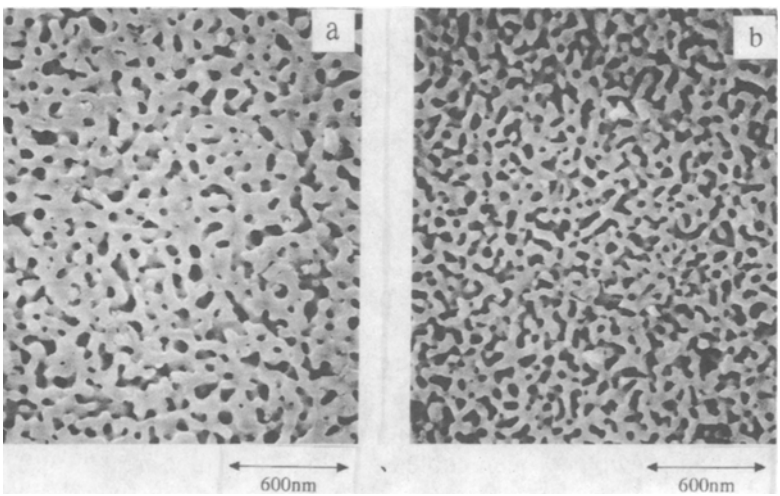

Fig. 1 Typical scanning electron micrographs of MPG300 (a), and MPG475 (b)

DSC measurements

The samples containing water were prepared by first immersing them in distilled, deionized water and then maintaining the system under reduced pressure to remove air trapped in the pores. About 5 mg of the sample saturated with water was hermetically sealed in a high-pressure aluminum crucible that was covered with aluminum oxide.

A Perkin-Elmer differential calorimeter model DSC-II attached to a cooling apparatus and equipped with a data processing system developed by the author was used to measure the melting and freezing curves of water in the MPG. All scans were conducted at a low scanning rate, 0.31 K min^{-1}, to avoid thermal and time delays in the DSC curve. The heat fluxes were calibrated using the heat of melting of the distilled water, while the temperature of the heating curve was calibrated using the onset temperature of the melting peak of the distilled

water. The temperature calibration of the freezing curve was carried out by extrapolating the melting onset temperature of the distilled water as a function of scanning rate to -0.31 K min^{-1}, because during cooling it is difficult to calibrate the temperature using crystallization of a standard sample due to supercooling. In addition, when the PSD curve was calculated from the DSC curves, the temperature calibration was performed for correcting thermal and time delays in a way similar to the purity analysis by DSC, in which the slope of melting of indium was utilized. The accuracy of the heat flux is estimated to be about ±3% or better. At the end of each DSC measurement, a small hole was made in the crucible and then it was dried under vacuum in an oven at 383 K for determining the mass of water.

The PSDs were calculated from the melting endotherms and the freezing exotherms using a computer program executed in Windows 3.1, which was written by the author with a Microsoft-C compiler and System Development Kits for Windows [1, 2].

Results and discussion

Freezing and melting behavior of pore water in MPG

Figures 2 through 4 show typical freezing and melting curves concerning water confined in the pores of MPG. The first cooling curves shown by the dotted and broken curves and the continued heating curves shown by the solid curves were measured over the temperature range of 284–225 K. Furthermore, the samples had previously been cooled to 225 K and then heated to 272.7 K.

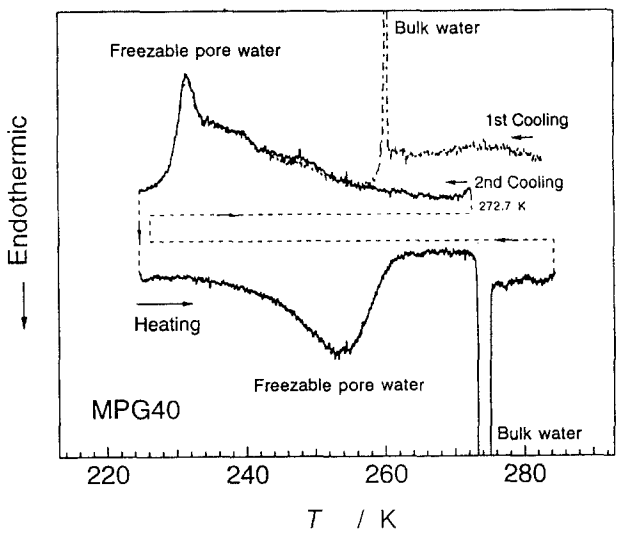

Fig. 2 The DSC curves of MPG40 saturated with water

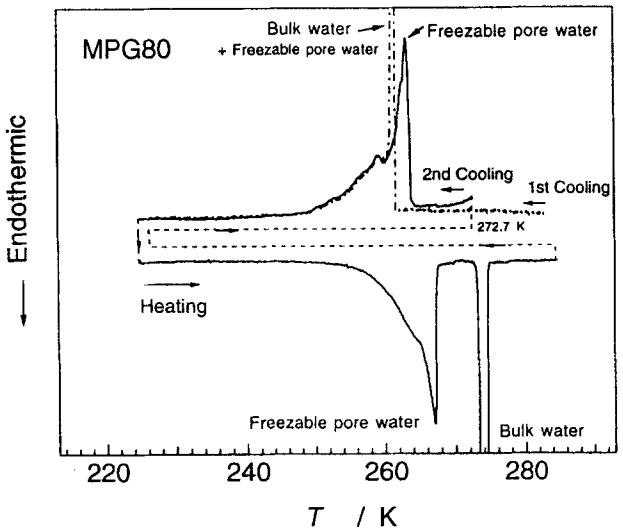

Fig. 3 The DSC curves of MPG80 saturated with water

After the thermal equilibrium, the second cooling curves shown by the solid curves were measured over the temperature range from 272.7 to 225 K to avoid significant supercooling.

Two distinct endothermic peaks were observed in the heating curves of all samples. The endotherms at the higher temperature are assigned to the melting of bulk water, while the endotherms at the lower temperature are assigned to the melting of freezable pore water in the pores of MPG. In contrast, the aspects of

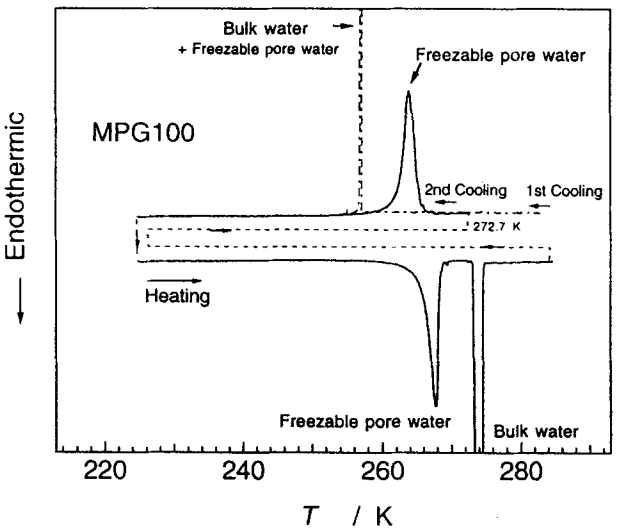

Fig. 4 The DSC curves of MPG100 saturated with water

the cooling curves depend considerably on the samples. The freezable pore water in the pores larger than the size of the primary nucleus of bulk ice was supercooled, but the freezable pore water in the smaller pores was not significantly supercooled. As illustrated in Fig. 4, an exotherm was not detected over the temperature range from 260 to 273 K in the first cooling scan for MPG100. However, in the second cooling scan, an apparent exotherm on the freezing of the freezable pore water present in the pores was observed in that temperature region. These findings suggest that the freezable pore water would be supercooled up to the freezing temperature of bulk ice unless the nucleus of the bulk ice was present and also that the size of the pores in MPG100 would be larger than the size of the primary nucleus of bulk ice as speculated from Eq. (1) because the freezable temperature of freezable pore water in MPG100 was higher than that of bulk water. For MPG80, as illustrated in Fig. 3, the freezing peak in the first cooling scan had a slow decay at lower temperatures, and the tail of the freezing curve was superimposed on that in the second cooling scan, although the tails of the freezing curves on the higher temperature side above the peak temperature were quite different. On the other hand, for MPG40, as illustrated in Fig. 2, the freezing peak of the freezable pore water appears even in the first cooling scan, which is located below the freezing temperature of bulk water and overlaps the freezing peak in the second cooling scan. Consequently, if the size of the pores is smaller than the size of the primary nucleus of bulk ice, it is concluded that significant supercooling of the freezable pore water does not take place. These findings above are essentially the same as those obtained with silica gels [1] and poly(methyl methacrylate) hydrogels [3].

Besides freezable pore water and bulk water as described above, the presence of nonfreezable pore water that seems to be present near the surface of the pores was revealed in MPG. The amounts of nonfreezable pore water were determined by subtracting the freezable water content from the total water content using the procedure reported in the previous paper [6].

Procedure for transformation of DSC curves to pore size distribution curves

The PSD curves were determined from the freezing and melting curves of freezable pore water via thermoporosimetry, following the procedure reported in the literature [2]. In the present study, the shapes of pores for MPG were simply assumed to be cylindrical, the same as used for silica gels [2] and for poly(methyl methacrylate) hydrogels [3].

For determination of the PSD curve, first the abscissa of the DSC curve, temperature T, is transformed into pore radius R [1] by the equation

$$R = \frac{\alpha(T)}{\Delta T} + \beta \tag{1}$$

where R is the pore radius, ΔT ($=T-T_o$; T_o is the triple point of water) is the depression of the melting or freezing temperature of the freezable pore water, and $\alpha(T)$ is a coefficient as a function of temperature which was determined to be $56.36\Delta T-0.90$ during freezing and $33.30\Delta T-0.32$ during melting in nm K [1, 2]. The first term on the right side of Eq. (1) represents the radius of freezable pore water, while the second term, β, is the thickness of nonfreezable pore water adsorbed near the surface of the pores, which was estimated by iterative optimization [2].

Subsequently, the ordinate of the DSC curve, heat flow, dQ/dt, is transformed into a derivative change of volume in the pores using the equation

$$\frac{dV}{dR} = \frac{dq}{dt}\frac{dt}{dR}\frac{1}{m\Delta H(T)\rho(T)}\frac{R^z}{(R-\beta)^z} \tag{2}$$

where V is the cumulative pore volume as a function of the pore radius, m is the weight of MPG, $\Delta H(T)$ is the enthalpy change in the melting or freezing of freezable pore water, which was assumed to be the same as that of bulk water as a function of temperature, and $\rho(T)$ is the density of the freezable pore water as a function of temperature, which was approximated as the density of bulk ice during melting and as that of supercooled water during freezing [1]. Moreover, z is defined as a factor of the shape of the pore, which equals 2.0 for a cylindrical pore and 3.0 for a spherical pore [1]. In the present study, the value of z was assumed to be 2.0.

The value of β was determined by repetitional optimization until the peak area of the PSD curve equaled the entire pore volume, V_p, calculated from the equation

$$V_p = V_{fp} + V_{nf} \tag{3}$$

where

$$V_{fp} = \int_0^\infty \left(\frac{dV_{fp}}{dR}\right) dR \tag{4}$$

$$V_{nf} = \frac{W_{nf}}{\rho_{nf}} \tag{5}$$

where V_{nf} is the volume of nonfreezable pore water, and ρ_{nf} is the density of nonfreezable pore water that is approximately similar to the density of bulk ice [6].

Pore size distribution of MPG

The typical PSD curves of MPG100 obtained via both thermoporosimetry and mercury porosimetry are shown in Fig. 5. The solid and dashed curves were determined by transforming the freezing and melting curves, respectively, shown in Fig. 4. Although noise spikes were observed in the PSD curve obtained via mercury porosimetry, the peak radius of the PSD curve was generally consistent with those obtained via thermoporosimetry. The noise may be associated with the pore shape, e.g., constricted in the middle.

All the PSD curves for MPG determined via thermoporosimetry are summarized in Figs 6 and 7. The peak radii of the PSD curves calculated from the freezing curves are generally consistent with those from the melting curves; whereas, the peak heights calculated from the freezing curves were slightly higher than those from the melting curves.

The thickness, β, of the layer of nonfreezable pore water determined by the optimization is tabulated in Table 1. The β values for MPG40, MPG80, MPG100, MPG145, MPG475, MPG750 and MPG1000 ranged from 0.2 to 1.2 nm, indicating that the thickness of the layer of the freezable bound water corresponds to 1–4 monolayers of water near the surface because the van der Waals radius of water is about 0.3 nm. On the contrary, the β values for

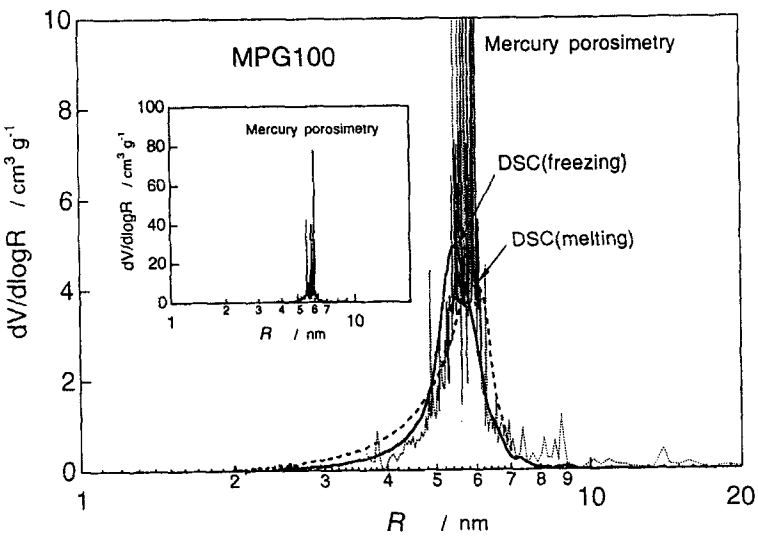

Fig. 5 The PSD curves determined via both thermoporosimetry and mercury porosimetry. The dotted curve represents the result of mercury porosimetry, and the solid and broken curves represent the PSD curves calculated via thermoporosimetry from the freezing and melting curves of water, respectively, shown in Fig. 4. The inside figure on the left-middle side is the PSD curve from mercury porosimetry on an expanded scale

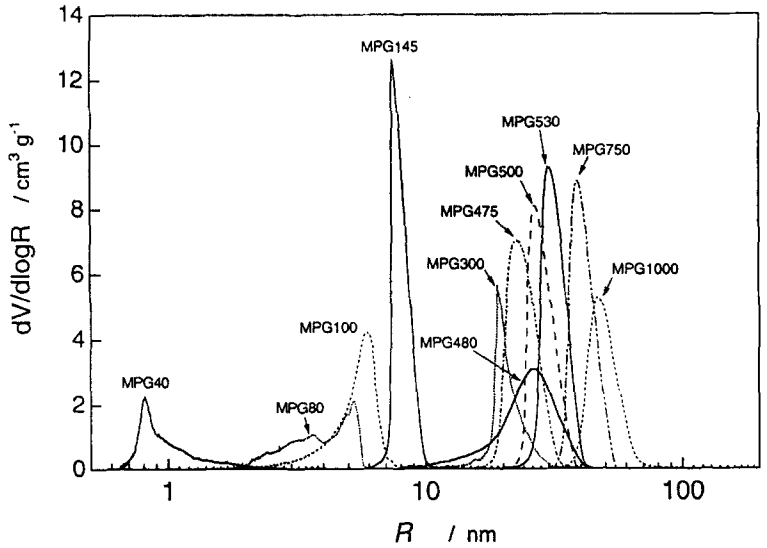

Fig. 6 The PSD curves determined from the freezing curves of water in MPG

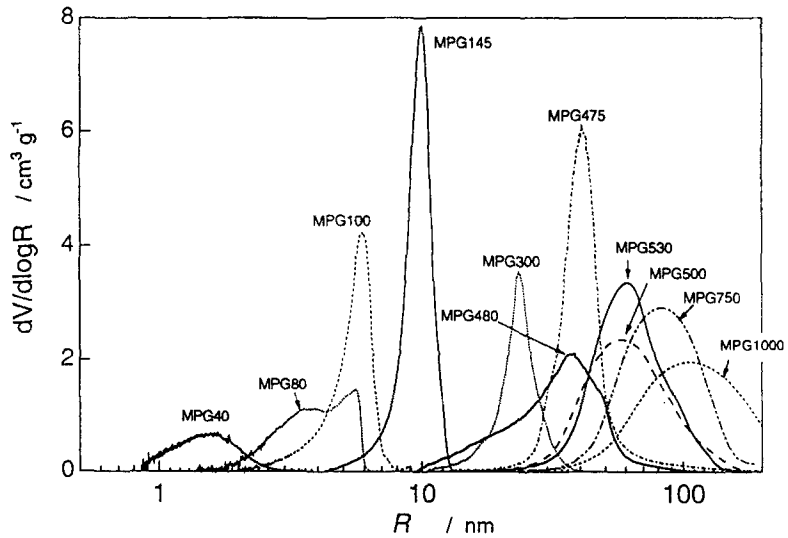

Fig. 7 The PSD curves determined from the melting curves of water in MPG

MPG300, MPG480, MPG500 and MPG530 ranged from 1.4 to 3.2 nm. The reproducibilities of the β were about ±10% or better; however, they would be too large because the hypothesis of two or three monolayers of adsorbed water on some materials has been proposed in the literature [6–11]. The origin of these extraordinary β values, in particular for MPG300, was speculated to be due to the presence of small pores less than 1 nm, because all of the water in

Table 1 Pore structures of MPG determined using mercury porosimetry and thermoporosimetry

Sample	Mercury porosimetry			Thermoporosimetry (DSC)						
				β /	Melting (heating scan)			Freezing (cooling scan)		
	$R_{mercury}$ / nm	$V_{mercury}$ / $cm^3\ g^{-1}$	$S_{mercury}$ / $m^2\ g^{-1}$	nm	R_{dsem} / nm	V_{dsem} / $cm^3\ g^{-1}$	S_{dsem} / $m^2\ g^{-1}$	R_{dscf} / nm	V_{dscf} / $cm^3\ g^{-1}$	S_{dscf} / $m^2\ g^{-1}$
MPG40	–*	–*	–*	0.36	1.7	0.200	276.0	0.8	0.294	617.0
MPG80	6.7	0.363	108.9	0.56	5.5	0.435	237.3	5.2	0.406	220.1
MPG100	6.1	0.599	196.9	0.44	5.9	0.622	243.8	5.5	0.545	207.6
MPG145	8.8	0.850	193.0	0.59	10.1	0.958	205.2	7.5	0.880	218.5
MPG300	16.1	0.415	51.5	3.18	23.6	0.512	45.4	19.2	0.484	47.2
MPG475	23.0	1.046	90.8	1.20	40.7	1.078	53.5	22.6	1.010	85.1
MPG480	20.5	0.791	77.2	2.44	37.5	0.790	54.4	26.3	0.756	65.3
MPG500	30.3	0.845	55.8	1.55	57.3	0.974	34.4	26.6	0.919	64.9
MPG530	32.9	0.986	59.9	1.37	61.5	1.115	38.2	30.4	1.033	65.4
MPG750	46.4	1.003	43.2	0.74	81.5	1.151	29.9	38.8	0.987	48.4
MPG1000	58.1	0.941	32.4	0.24	104.8	1.031	21.7	47.1	0.714	29.3

* Mercury porosimetry could not be applied to MPG40 because the pores were too small

the small pores should become nonfreezable pore water. If these small pores are present, the β must be estimated to be too large using the algorithm of the optimization. In any case, the errors in the peak radii of the PSD curves that arise from the errors in the estimation of β are less than 20%.

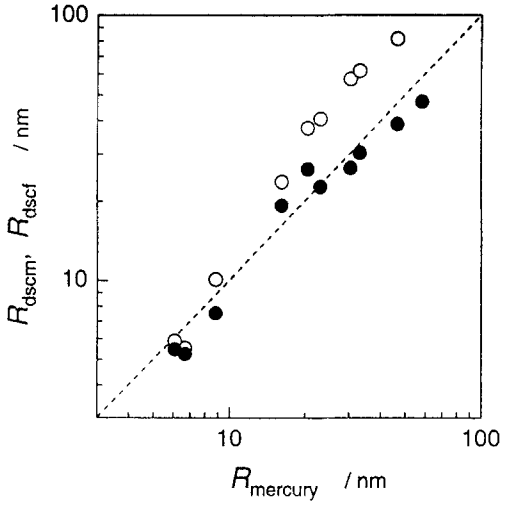

Fig. 8 The comparison of pore radii obtained via both thermoporosimetry and mercury porosimetry. The open and closed circles represent R_{dscm} and R_{dscf}, respectively

The peak radii, R_{dscm} and R_{dscf}, of the PSD curves obtained from the melting and freezing curves, respectively, and the average radii, $R_{mercury}$, obtained via mercury porosimetry are also tabulated in Table 1, and the relationships among the pore radii are shown in Fig. 8. At first glance, R_{dscf} was found to be consistent with the $R_{mercury}$. The R_{dscm} was in good agreement with both $R_{mercury}$ and R_{dscf} regarding MPG that has pores less than 10 nm in radius. However, the R_{dscm} was larger than both $R_{mercury}$ and R_{dscf} regarding MPG that has pores more than 20 nm. This difference would originate in the thermal and time delays in the DSC melting curves, as reported in the previous paper concerning silica gels [2]. Based on the above findings, it is concluded that thermoporosimetry can determine pore sizes of less than at least 58 nm; however, it seems to be difficult to determine with high accuracy the PSD curve more than 20 nm from the melting curve measured at a scanning rate of 0.31 K min^{-1}.

The relationships among the pore volumes, V_{dscm} and V_{dscf}, evaluated via thermoporosimetry from melting and freezing, respectively, and the pore volume, $V_{mercury}$, evaluated via mercury porosimetry are shown in Fig. 9. The pore volumes of V_{dscm} and V_{dscf} were found to be in good agreement with $V_{mercury}$, similar to the findings obtained for silica gels [2].

In addition to the pore radii and the pore volumes, the surface areas of the pores in MPG were calculated from the PSD curve using the equation

$$S = \int \frac{z}{R} \left(\frac{dV}{dR} \right) dR \tag{6}$$

The calculation results are also listed in Table 1. Here S_{dscm} and S_{dscf} refer to the surface areas calculated using the PSD curves obtained from the melting and freezing curves, respectively. Figure 10 depicts the results for S_{dscm} and S_{dscf} cal-

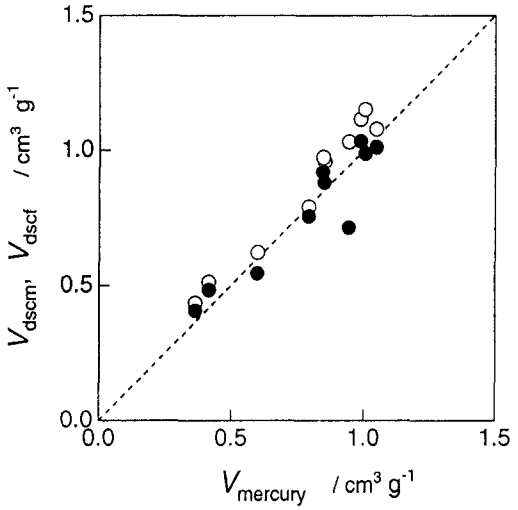

Fig. 9 The comparison of the cumulative pore volumes determined via both thermoporosimetry and mercury porosimetry. The open and closed circles represent V_{dscm} and V_{dscf}, respectively

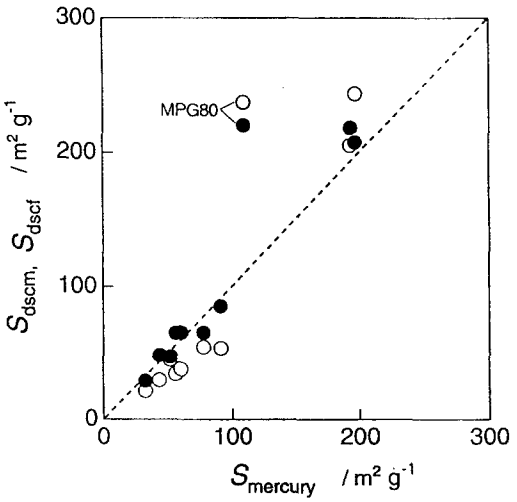

Fig. 10 The comparison of the surface areas determined via both thermoporosimetry and mercury porosimetry. The open and closed circles represent S_{dscm} and S_{dscf}, respectively

culated as $z = 2.0$, plotted against $S_{mercury}$. For MPG80, both S_{dscm} and S_{dscf} were quite a bit larger than $S_{mercury}$, which would be associated with the difference in the shape of the PSD curves; *i.e.*, as shown in Figs 6 and 7, the double peaks in the PSD curves of MPG80 were detected by thermoporosimetry, while only single peak in the PSD curve was detected by mercury porosimetry due to being beyond the limit of measurement of mercury porosimetry. On the contrary, for all MPG except for MPG80, both S_{dscf} and S_{dscm} were quite consistent with the $S_{mercury}$.

Conclusion

The pore structure for microporous glass was determined via both thermoporosimetry and mercury porosimetry. The pore radii, the pore volumes and the surface areas determined via thermoporosimetry were in good agreement with those determined via mercury porosimetry. Thermoporosimetry has proved to be an effective technique for determining pores less than at least 58 nm.

References

1. K. Ishikiriyama, M. Todoki and K. Motomura, J. Colloid Interface Sci., 171 (1995) 92.
2. K. Ishikiriyama and M. Todoki, J. Colloid Interface Sci., 171 (1995) 103.
3. K. Ishikiriyama, M. Todoki, T. Kobayashi and H. Tanzawa, J. Colloid Interface Sci., 173 (1995) 419.
4. K. Ishikiriyama, A. Sakamoto, M. Todoki, T. Tayama, K. Tanaka and T. Kabayashi, Thermochim. Acta, in press.
5. T. Nakashima, Papers published in Commemoration of 3rd Anniversary of SPG Application Technique Society, 1989, p. 10.
6. K. Ishikiriyama and M. Todoki, Thermochim. Acta, 256 (1995) 213.
7. M. Brun, A. Lallemand, J. F. Quinson and C. Eyraud, Thermochim. Acta, 21 (1977) 59.
8. Y. P. Handa, M. Zakrzewski and C. Fairbridge, J. Phys. Chem., 96 (1992) 8594.
9. W. Drost-Hansen, Ind. Eng. Chem., 61 (1969) 10.
10. A. A. Antoniu, J. Phys. Chem., 68 (1964) 2745.
11. G. G. Litvan, Can. J. Chem., 44 (1966) 2617.